Non-Contact Articulated Robot-Integrated Gap and Flushness Measurement System for Automobile Assembly

IEEE Access
Multidisciplinary | Rapid Review | Open Access Journal

Received 11 July 2022, accepted 5 August 2022, date of publication 16 August 2022, date of current version 23 August 2022.

Digital Object Identifier 10.1109/ACCESS.2022.3199066

RESEARCH ARTICLE

Non-Contact Articulated Robot-Integrated Gap and Flushness Measurement System for Automobile Assembly

JASURKHUJA KHOLKHUJAEV[1,2], GIACOMO MACULOTTI[2], GIANFRANCO GENTA[2], MAURIZIO GALETTO[2], AND JAMSHID INOYATKHODJAEV[1]

[1]Department of Mechanical and Aerospace Engineering, Turin Polytechnic University in Tashkent, Tashkent 100095, Uzbekistan
[2]Department of Management and Production Engineering, Politecnico di Torino, 10129 Turin, Italy

Corresponding author: Jasurkhuja Kholkhujaev (jasurkhuja.kholkhujaev@polito.it)

ABSTRACT The paper proposes and metrologically characterizes a gap and flushness optical measurement system based on machine vision. The system is developed for an operator-free application as a plug-and-play feature for articulated robotic arms. The system is designed for use in Stop-and-Go quality control point of vehicle assembly process. Non-contact measurement system that consists of an ultraviolet line laser with a sensitive camera and complemented with an advanced machine vision measurement algorithm is developed. The system is directly calibrated according to state-of-the-art literature and the measurement uncertainty within the laboratory conditions is derived according to Guide to the Expression of Uncertainty in Measurement. Measurements on the real vehicle body is done to elicit the difference. The expanded uncertainty achieved by the system is 0.221 mm and 0.177 mm for gap and flushness respectively, significantly smaller than the sole resolution of the most adopted manual feeler gauge verification method.

INDEX TERMS Gap and flushness, non-contact measurement, line laser system, camera calibration, machine vision, body-in-white.

I. INTRODUCTION

The importance of vehicle body structure is a crucial factor influencing the automobile body exploitation [1]. Structural frame of an automobile body must be designed in the way that the dimensional variability of the assembled parts should not create criticalities related to wind noise, water leakage, door closing effort, gap and flushness variations. Henceforth, ensuring good mating and adequate quality control, to keep within tolerances interfaces and related geometrical dimensions, e.g., gap and flushness, is essential for high comfort, noise-vibration-harshness (NVH) performances, low aerodynamic drag and respect some core voice of customer requirements, e.g., low noise and effort in closing doors. The quality of vehicles body in industry is controlled through a time-consuming methodology of measurements during the production process [2], [3]. The measurement of the gap and flushness in vehicle assembly is one of the key points of body exterior quality control process. The gap is the horizontal difference between two surfaces on the body of the automobile, while the flushness is the vertical height that is perpendicular to those surfaces, as shown in Figure 1. The gap and flushness are the main points of interest for many customers as they give a first impression on the quality of the vehicle produced. Hence, they directly influence perception of the vehicle by customers and therefore the sales [4]. Today, automotive design focuses on optimizing the trade-off between the aesthetic look and reducing the aerodynamic resistance with free-form shapes on the gaps. Manual methods of gap and flushness measurements often does not have adequate metrological performances to verify the designed tolerances [5]. Furthermore, as in many vehicles' assembly points, the measurements are performed manually, and it is almost impossible to gather continuous data. Typically, the gap and flushness measurement data are collected only if the result are beyond the admissible variability tolerance of

The associate editor coordinating the review of this manuscript and approving it for publication was Shih-Wei Lin.

the factory, or in the quality control points where randomly chosen vehicles are fully analyzed. Conventional gap and flushness measurements also have a number of different disadvantages, for they are based on mechanical contact with the surface of the vehicle and may deform the gaps.

The measurement is highly dependent on the positioning of the mechanical measurement devices and the qualification of the operators using the tools. As shown in the Figure 1, the gap and flushness are measured with feeler gauges that have, in the best-case scenario, a resolution of 0.25 mm at Body Shop quality check point of the car body.

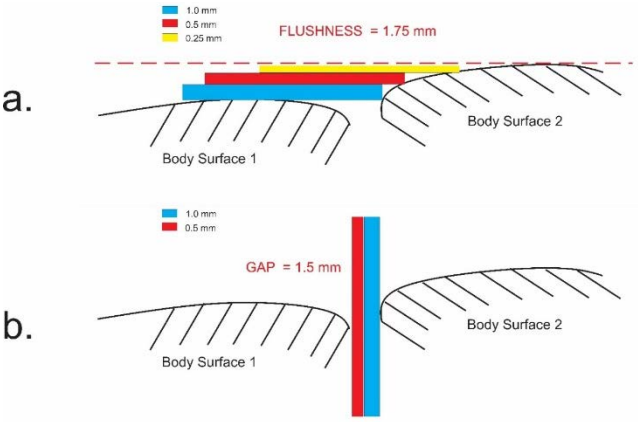

FIGURE 1. Manual method of gap and flushness measurement a) flushness measurement b) gap measurement.

A number of different approaches have been defined to measure the clearance between the surfaces on the automobile by automatic or semi-automated measurement methods. Laser reflection [6], [7] and ultrasonic methods [8] are non-contact measurement methods that have been developed, alternative to gauge-based approaches. Laser and ultrasonic reflection methods differ in the nature of the emitted source, i.e., the first uses the laser whilst the ultrasonic approach the sound [9]. These methods rely on the knowledge of the travel speed of the wave in air and the reflection of the wave from the object surface to calculate the distance, known the time-of-flight. However, both methods have high uncertainty, which increases as the distance to the measurand object surface increases. A more recent approach is a laser vision-based technique that provides better precision and is less dependent on the reflection of the object. Laser-vision systems mainly exploit laser-triangulation method [10], [11], [12]. Also, a stereo camera-based approach has been developed to solve the issues with color dependency of other alternatives [13]. Semi-automated techniques are used to enable operators to use simpler available tools, like smartphones. The first attempt was the Samsung Galaxy Beam® that features a small projector connected on top of the smartphone that projects a pattern on the measurand [14]. Unfortunately, the system is suitable only for this type of smartphone that is now out of production. An update and generalization of the technology has been conceived by the GOOD MAN

FIGURE 2. Feeler gauges used in the production process for measurement of car body.

project [15], which developed smartphone-based gap and flushness measurement system based on Raspberry Pi and Pi-Cam camera. Today commercial market is also rich of diverse products like GapGun [16], LMI company Laser Gauge [17] and Calipri by Hexagon [18]. However, manual commercially available tools results in time consuming measurements, whilst available automated systems are too expensive to be used in quality control of each car in mass production vehicle assembly processes, while they can be used in premium car production lines. Therefore, in mass production, manual gauge measurement system that only enables a GO/NO GO test is adopted to verify the product with respect to factory specifications. Accordingly, the current measurement procedure in the production process by an operator consists in putting feeler gauges or dial gauges, shown in Figure 2, with resolution of 0.25 mm at painted car body quality control point. The measurement is taken based on the vertical insertion inside the gap and on the visual feedback of the operator. The latter tries to insert the gauge and measure as much vertical as possible in order to obtain correct orientation.

This paper proposes an innovative a high-speed non-contact measurement system that is integrated into a robotic arm. The system consists of the laser light source with the complementary metal-oxide semiconductor (CMOS) camera. The line laser is mounted as end effector of the articulated robot, on which a frame is attached to. The frame is exploited to mount the camera to allow the vision system to be moved and acquire data with a fixed relative position with respect to the line laser. The system is completed by an automated machine vision image processing algorithm, run on the remote PC with the USB 3.0 connection to camera. The system is designed for measurement of gap and flushness of the painted car body, i.e. the assembly featuring the Body In White (BIW) and the doors, after the painting operation. The system is proposed as the moving platform for Stop-and-Go system.

The proposed gap and flushness measurement system aims at providing a cheap, accurate and precise automated measurement of the car body, that is also capable of significantly reducing the operators' error.

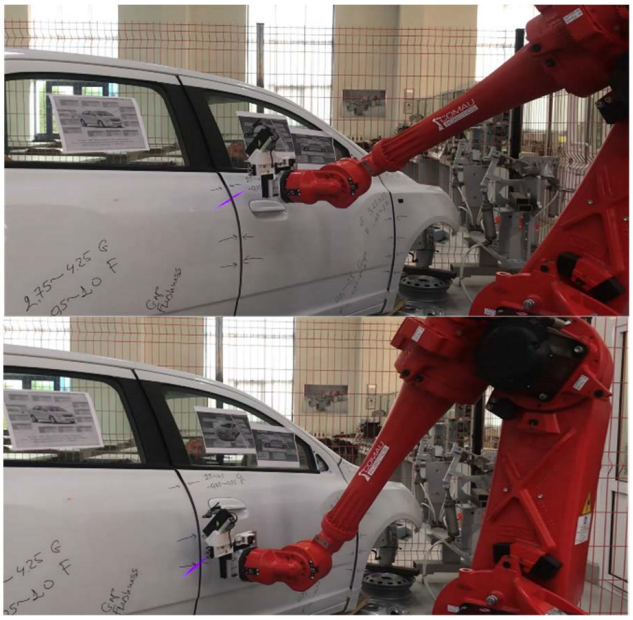

FIGURE 3. The designed system in operation, notice the purple laser line. The system is represented in a R&D laboratory; for confidentiality the image of the system in the production plant cannot be shown.

Hence, the main contribution of the system is the integration of gap and flushness measurement methodology to the robotic arm systems. The system is designed in the most simplified form with just a camera and mono-line laser [19], [20] and complemented by a machine-vision algorithm. The system is calibrated and validated to ensure traceability and metrological performances of the measurement system.

The rest of the paper is organized as follows. Section 2 discusses the hardware design. Section 3 analyzes the software and image processing algorithms. Section 4 describes the calibration methodology of the developed system. Section 5 discusses the metrological characterization and validation of the system. Finally, Section 6 presents the conclusions and future perspectives.

II. MEASUREMENT SYSTEM HARDWARE DESIGN

The system consists of a line laser end effector complemented by a camera system for machine vision mounted on a frame attached to the articulated robot, as shown in Figure 3. Laser line projected onto the surface and the camera image processing is a commonly known technique for 3D scanners. Typically, laser triangulation method is used to calculate the distance to the object by the help of precise measurement of the angle between the camera and laser light. However, the accurate knowledge of relative position is necessary for 3D scan of components, which is not the considered scope. In fact, considering that the proposed system features a fixed relative position between the camera and the line laser, and that these two are moved rigidly, it is only required to calibrate the camera pixel coordinates with respect to the horizontal gap and vertical axis parallel to normal of the surface.

In the present work, the target surface is the painted car body. The measurements are carried out in the laboratory Stop-and-Go point inside the room where no light is allowed. This particular environmental condition aims to decrease the signal to noise ratio and the noise from the factory light sources. Additionally, this particular set-up minimizes any possible influence of the paint color. In order to be able to see the points where the laser light is emitted, first the robotic arm is programmed inside the factory light. During the measurements, the door gap and flushness are considered.

The laser system is aimed at measuring painted car after the paint shop where the plastic feeler gauges practically used have a resolution of 0.25 mm. The surface is crucial factor influencing the reflectance of the laser light. The body of the vehicle that has to be measured is a smooth surface with a small roughness, typically assessed in terms of Ra. However, Ra values that are close to the light source wavelength can influence substantially the laser light scattering [21]. Also, the laser should be visible to enable easy programming of the robot and detection by the machine vision system camera. Accordingly, the choice of the laser light source falls on the shorter wavelength in the visible spectrum. Visible ultraviolet laser is a convenient choice, for it meets all the previous requirements and, with respect to other possible alternatives, i.e., dominated by green or red components, it presents a lower scatter. Accordingly, the laser light source was chosen with a wavelength of 405 nm and 5 mW power.

This laser source should enable the camera sensor and lenses to acquire in ultraviolet spectral region between 200 nm to 400 nm. The camera used in this research is Basler ace acA2500-14uc with 1/2.5 CMOS progressive scan sensor and resolution of 2590 $\times$ 1942 pixels with good spectral response in violet region (Quantum efficiency of 35% at 405 nm). Camera uses Basler lens, a fixed focal length of 8.0 mm, F-stop settings from F1.8-F22 and resolution of 5 megapixels. In order to assess the scale factor, i.e. the physical pixel-to-millimeters ratio, within the working range of camera, the camera resolution pixel-per-mm analysis will be calibrated, and methodology and results of the calibration are addressed in Section 4. As mentioned, the system features a frame attached to the articulated robot to allow mounting of the camera.

The system is designed to operate in the distance of about 60-100 mm from the object and about 100-150 mm from the camera inclined with respect to the laser emitter axis. The laser fan angle is 55°.

The relative position between the line laser and the camera is critical, for it determines possible alignment errors in the measurement of the gap and flushness. Two alternatives are available according to the literature, and as depicted in Figure 4: i) camera orthogonal to the surface and inclined laser (as per Figure 4.a and Figure 4.a-a) or ii) line laser orthogonal to the surface and inclined camera (as per Figure 4.b and Figure 4.b-b).

If the system is based on the solution as in Figure 4.a and Figure 4.a-a, problem arises in obtaining the correct

data on the gap and flushness. In fact, because the laser is inclined with respect to the object, the gap and flushness will be obtained on the inclined planes. Therefore, projection on the orthogonal plane is required to estimate correct dimension. This requires additional system characterization and calibration, data analysis steps, and contribute non-negligibly to measurement uncertainty. Additionally, with this setup, the amount of light on the camera sensor due to highly reflective objects, as is the painted car body, would be small, thus decreasing signal-to-noise ratio. Conversely, in the case of laser fan is projected orthogonal to the object surface, as in Figure 4.b and Figure 4.b-b, these issues are inherently solved, at the cost of a loss of camera sensitivity in the vertical direction. Also, the second solution is consistent with industrial best practices and conventional use of feeler gauges. In fact, measurement with the gauges is typically performed with a vertical application of the gauges and a side inspection. According to this discussion, the camera and laser orientation are based on the second methodology, shown in Figure 4.b, which mimics up to a certain extent the best practices applied to measure the gap and flushness in the production facilities.

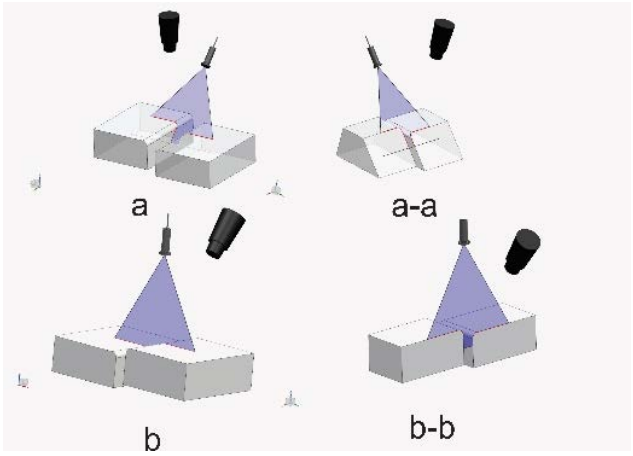

FIGURE 4. The laser and camera orientation a) camera is perpendicular, b) camera inclined with respect to laser, a-a) and (b-b) cross-section on the line laser plane.

The relative orientation of the camera with respect to the plane, i.e., the angle ϑ in Figure 5, is critical to optimize the imaging to allow a fast and robust measurement of the gap and flushness. The more the camera is aligned with the laser plane, i.e., the smaller the angle ϑ, the less sensitive the camera is in along the z_O coordinate axis of Figure 5. Accordingly, the ideal scenario to measure the flushness would feature a camera oriented at $\vartheta = 90°$ with respect to the line laser plane. However, such design is not compatible with the general accessibility of the automobile body. Consequently, the angle has to be significantly reduced. Additionally, for the considered surface application, the literature [21] reports that the inclination angle affects the sensitivity to light scatter of the camera acquired images. These are minimized for angles in intermediate position. Moreover, working distances of the camera and the laser represents two major

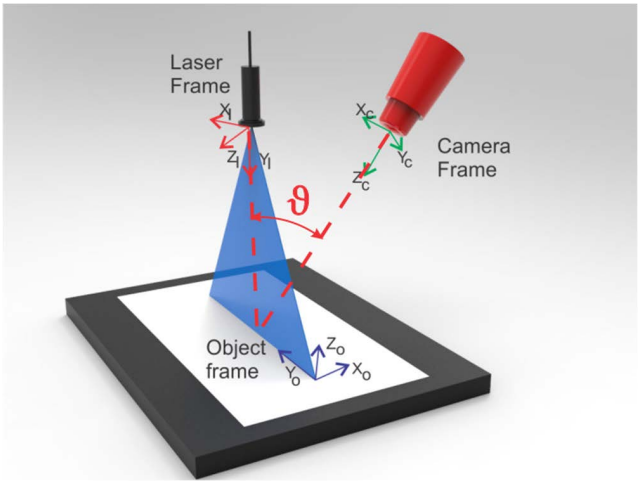

FIGURE 5. Laser-camera frame.

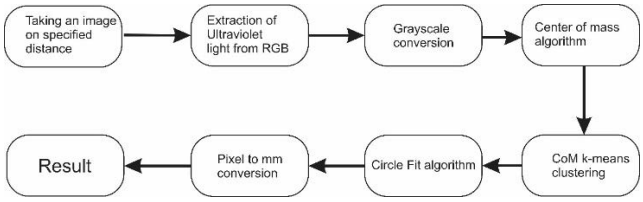

FIGURE 6. Algorithm of proposed gap and flushness measurement system.

constructive constraints to the system design. Additionally, a desirable feature is to have a highly focused laser line which occupies the largest portion possible of the camera field of view. Accordingly, preliminary experiments were conducted testing different orientations with the angle ranging from 20° to 60°. The optimal condition resulted the solution featuring a relative orientation $\vartheta = 60°$ with respect to the laser line plane.

III. MEASUREMENT SYSTEM

The aim of the gap and flushness measurement system here proposed is to extract the laser light from the image, based on image processing algorithms, whose workflow is reported in Figure 6.

The camera feed is run through Python algorithm in a general-purpose PC (i5 Processor) with plugin feature of the Basler camera. Every process step is controlled by the PC. The camera sensor feature adjustment plays a key role in acquiring low noise image. The exposure time is set to 805 μs and Gamma adjustment to 3.99998 in order to obtain an image only showing the laser light. The acquired image is a pixel matrix of I columns and J rows.

A. ULTRAVIOLET LIGHT EXTRACTION AND RGB CONVERSION

The picture is first converted into the gray scale. Amongst the several methods to convert an image into grayscale [22]. Standard conversion from RGB to grayscale image exploits the

luminance as conversion parameter to match human brightness perception by using a weighted combination of RGB channels with a sum of weights to equal to unity [23]:

$$G_{Luminance} = 0.3R + 0.59G + 0.11B \tag{1}$$

This value is used throughout a number of image processing tools based on the perception of the human eye. However, in the case at hand, the laser is in the region of ultraviolet light, featuring a dominant blue component. Conversely, the luminance method of conversion of RGB image, in Eq. (1), gives more weight to the green and red color than blue, as can be seen from the values 0.59, 0.3 and 0.11, respectively, in Eq. (1), resulting in poor detection of the laser line, as depicted in Figure 6a.

The gray scale conversion aims at optimizing the identification of the intensity regions for the laser light. Therefore, to give more weight to the blue light spectrum, which is necessary to better detect ultraviolet laser source, a combination of the weight parameters of standard luminance algorithm on the conversion was proposed.

Maximum weight parameter according to the (1) in luminance algorithm is given to green spectrum with the value of almost 0.6, that is used instead for blue spectrum in (2) and equally dividing the rest 0.4 weight to red and green spectrum. The other way was to take the minimum parameter from (1) that is 0.11 and use them for both green and red spectrum to leave 0.78 to the blue spectrum, as it is done in (3).

$$G_{RedandGreen} = 0.2R + 0.2G + 0.6B \tag{2}$$

$$G_{Ultraviolet} = 0.11R + 0.11G + 0.78B \tag{3}$$

The Equation (2) and (3) applied to the RGB image can be seen in Figure 7.b and Figure 7.c, respectively, showing a decisive improvement in the detection of the laser, with respect to the standard conversion of (1), shown in Figure 7.a. In fact, assigning higher weight to the blue content optimizes the ultraviolet spectrum detection.

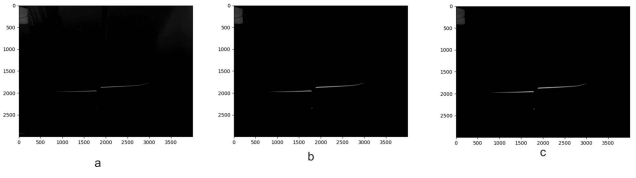

FIGURE 7. 5 Gray scale conversion algorithm application (a)- G_Luminance (b)- G_(Red and Green) (c)- G_Ultraviolet.

In order to have better view, we could look closer in Figure 7 at the region of interest, i.e. where the gap and flushness are, in Figure 8. Region of interest of the grayscale converted pictures in Figure 8.a represents standard luminance algorithm and Figure 8.b, Figure 8.c for "red and green" and blue, i.e., ultraviolet, equations respectively. As can be seen from Figure 8.c with the largest weight on the blue, the ultraviolet can be extracted with better resolution. Therefore, the (3) will be used to work with grayscale image.

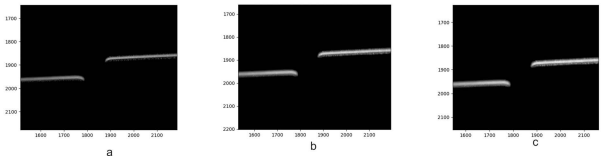

FIGURE 8. Region of interest zoomed view for grayscale (a)- G_Luminance (b)- G_(Red and Green) (c)- G_Ultraviolet.

B. CENTER OF MASS ALGORITHM

The center of mass (CoM) algorithm is applied to the system in order to extract the peak intensity of the laser light from the grayscale image. In this system, where the measurement accuracy plays an important role, the scope of the system relies on the location of particular point on the picture. The location of the peak intensity is determined according to the max intensity of each i-th column:

$$CoM_i = \frac{\sum_{j=L_{bound}}^{U_{bound}} I\,(j,i) * j}{\sum_{j=L_{bound}}^{U_{bound}} I(j,i)}, \tag{4.1}$$

$$L_{bound} = max\,\{I(\cdot,i)\} - k_1 \cdot s_{difference} \tag{4.2}$$

$$U_{bound} = max\,\{I(\cdot,i)\} + k_1 \cdot s_{difference} \tag{4.3}$$

where, I(j,i) is the intensity of the pixel at the j-th row and i-th column. $s_{difference}$ controls the scanning integral based on the Gaussian distribution of the laser intensity, which ranges from several pixels to tens of pixels. The laser dispersion differs from column to column. The factor $k_1 \cdot s_{difference}$ aims at reducing the computational effort by focusing on a tight neighborhood of the maximum. The $s_{difference}$ was experimentally taken as half of the maximum range of dispersion on the different columns. The coefficient k_1 is set to 2, to focus on a neighborhood of the laser intensity covering about 95% of the laser scatter. Results of the CoM algorithm is shown in Figure 9. However, as it can be noticed, noise and sparse data can affect the results. Therefore, outlier management method is applied in order to detect and remove the outlier and the additional contours on the picture [24], [25].

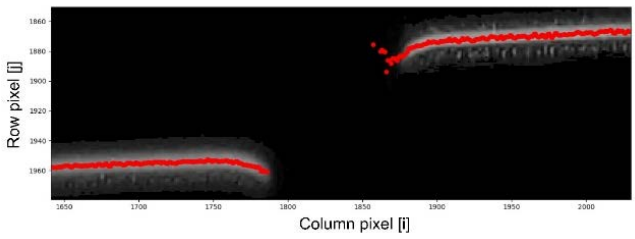

FIGURE 9. Center of mass algorithm application on the threshold intensity.

Accordingly, outermost region of the imaged laser line, which are irrelevant to the gap and flushness measurement, are cropped. Cropping is performed by a statistical approach to focus on the region with the higher probability of signal-bearing pixels. The mean and the standard deviation of the CoM_i set, i.e. including the CoM of

the different columns, are:

$$m = \frac{\sum CoM_i}{N} \tag{5.1}$$

$$s = \sqrt{\frac{\sum (CoM_i - \mu)^2}{N-1}} \tag{5.2}$$

Consequently, outermost region of the imaged laser line can be identified exploiting a confidence interval to highlight values outside it, with boundaries:

$$U_{outlierlimit} = m + dev_{max} \cdot s \tag{6.1}$$

$$L_{outlierlimit} = m - dev_{max} \cdot s \tag{6.2}$$

where the dev_{max} allows setting the confidence level covered by the confidence interval. The choice here exploited, according to common practices, seek for a 95% confidence level by setting the dev_{max} to 2.

The result of data obtained applying the CoM algorithm on the intensity and applying the outlier detection is shown in Figure 10.

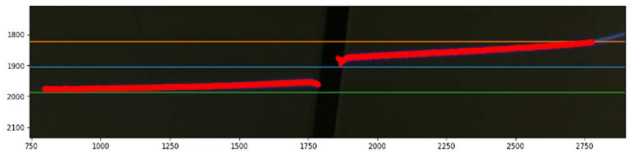

FIGURE 10. Mean value with upper and lower threshold.

C. k-MEANS CLUSTERING

Once the data have been filtered from noise and peak intensity has been identified, the data should be organized into two groups, representing the two facing metal sheet, to analyze and apply circle fitting algorithm separately on the two facing end. To perform this operation clustering algorithm is implemented [26]. In particular, k-means method is applied [27], [28]. It is one of the most widely used clustering technique that seeks to minimize the average squared distances between points in the same cluster. The main reason of applying the k-means algorithm for clustering is the simplicity and speed of execution. The basic algorithm for k-means clustering is as follows:

1. Randomly choose the k initial centers C = {c_1, c_2 . . . .., c_k}
2. Populate any cluster C_i i = {1, . . . k}, to be the set C_i of points of the dataset X that are closer to c_i than they are to c_j for all i≠j
3. For any i = {1, . . . k}, set c_i to be the center of mass of all points in C_i:

$$c_i = \frac{1}{|C_i|} \sum_{x \in Ci} x$$

4. Iteration of the step 2 and 3 until C no longer sensibly changes in value

It is standard practice to choose the initial centers randomly from X. Then, Step 2 and 3 both guarantee the decrease of distance until the distance between former and newly identified centers does not decrease sensibly anymore; however, the method is liable to find local minima.

In the considered case for gap and flushness measurement, based on image processing aimed at the laser line extraction, an improvement of the conventional k-means algorithm is proposed to have faster and more robust response to the clustering of the data. Because the laser line is almost centered with respect to the field of view and it is inherently split in two groups, the initialization can be performed exploiting those a-priori information.

Accordingly, the initialization of the first initial centroid is performed by finding the center of mass for our filtered data and accordingly splitting the dataset by column coordinates to half. In order to find the center of the coordinates, the CoM algorithm for column and row coordinates is implemented:

$$col_{center} = \frac{\sum filtered\_data[col]}{N} \tag{7.1}$$

$$row_{center} = \frac{\sum filtered\_data[row]}{N} \tag{7.2}$$

The data obtained from the col_{center} and row_{center} can be seen as the green star in Figure 11.

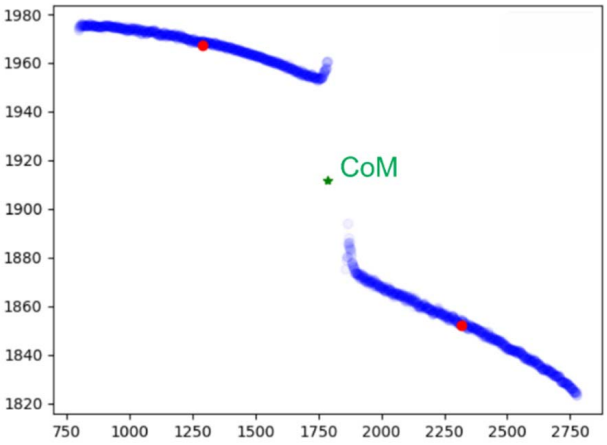

FIGURE 11. Center of mass algorithm application on the threshold intensity.

The center of mass computed thanks to (8) is almost in the middle of two data clusters. From this point onwards, the initial centroid can be computed for the data, by the CoM algorithm applied to the two cluster of columns, to fast initialize the clustering algorithm.

The next step defines the initial centroid for future 2 clusters of data. The algorithm that is used to find the centroid follows the simple rule shown in Figure 12, where the CoMg is the global CoM, computed by (8), whilst CoMi is calculated for values smaller and greater than CoMg shown in Figure 11.

Application of this technique results in fast response of a clustering system as can be seen by comparing Figure 13 and Figure 14.

The proposed approach, that non-randomly initializes the centroids, allows a significant reduction of computational

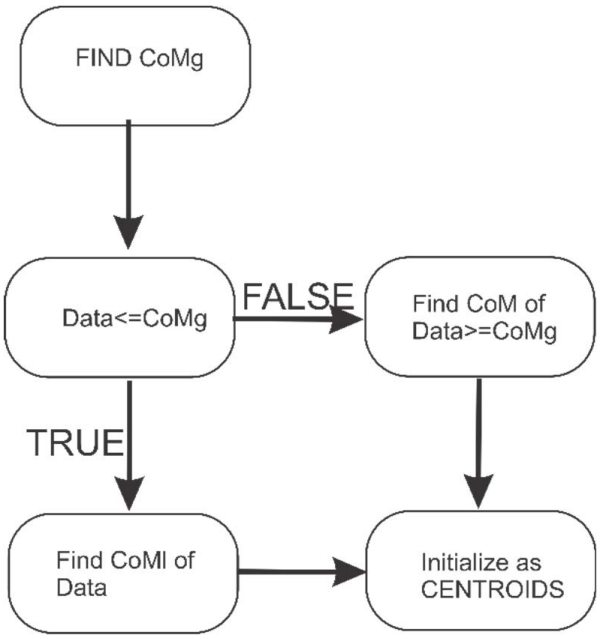

FIGURE 12. Algorithm for new k-means clustering.

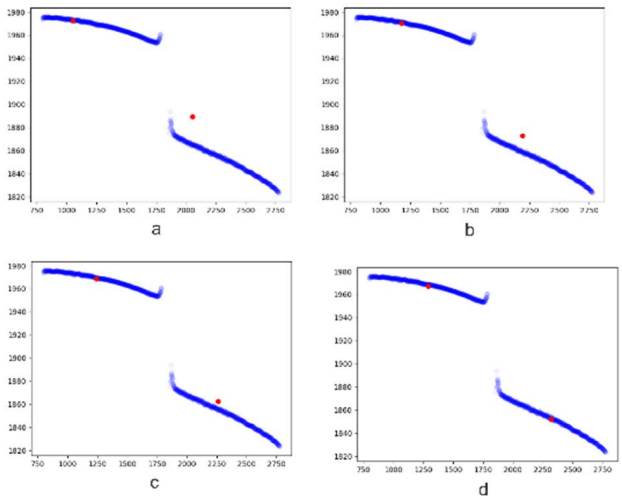

FIGURE 13. The classic k-means clustering with initial centroid randomly chosen a) 1st initialization b) 2nd iteration c) 3rd iteration d) 4th iteration.

effort. Also, it provides benefits over the classical k-means in terms of time, which is important when the system needs to compare and cluster a large number of images and a large number of filtered data. Figure 13, Figure 14 and Figure 15 report the comparison analysis between the classical algorithms and new method to define the initial centroids.

The random initialization of centroid in Figure 13.a already gave a result that is quite near to the data for one of the two cluseters. However, the random number initialization is quite unpredictable that could take a big number of iterations.

As one can see, the proposed method for k-means clustering for gap and flushness extraction need smaller number of iterations for calculation of centroids, thanks to the information-rich initialization.

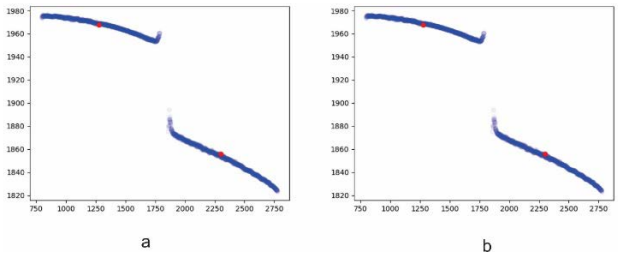

FIGURE 14. The proposed method a) Initialization b) 2nd (and last) iteration.

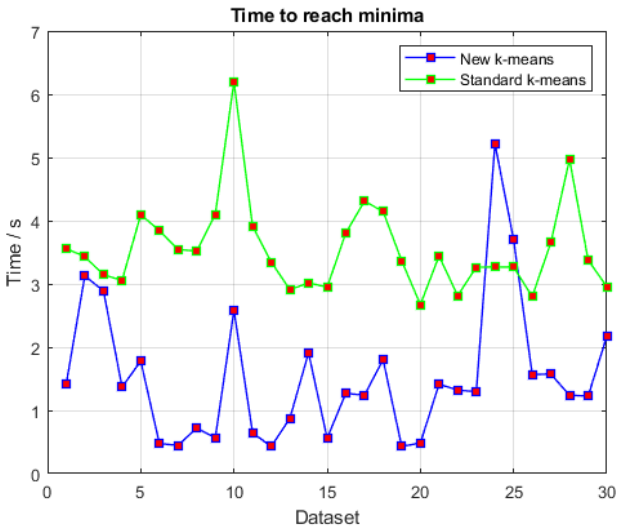

FIGURE 15. Center of mass algorithm application on the threshold intensity.

In particular, the algorithm is tested on 30 sample measured points, where gap and flushness could be measured. The algorithm with the new k-means clustering is faster than the standard k-means as shown in the Figure 15. Only for measured points 24 and 25 the values are higher that might be a reason of additional computation effort due to other processes in the machine. The average difference of computation with the Intel® Core™ i5-7200U Processor (3M Cache, up to 3.10 GHz) is enough to deduce that new k-means consumes less amount of time. The standard clock() operator is used to calculate computation time necessary for process to be executed in Python.

It is relevant to mention that, because k-means clustering depends on the available points, the cropping operation, introduced in Section 3.2, is essential to avoid that the tails far from the measured clearance bias the clustering results In that matter, different points on the automobile may impact on the measurement robustness, for, depending on the points position, the gap and flushness visibility is slightly different.

D. GAP EXTRACTION

Based on the clustering algorithm k-means, all the necessary data that could be used to apply the gap extraction algorithm were identified. The gap is measured based on the classical method of circle fitting [29].

A slightly different approach with respect to classical method of circle fitting is here proposed. After clustering the data into the left and right clusters on the body of the vehicle, it is important to get the minimum possible points that are needed to be extracted to reduce the computational effort of the fitting, without affecting the robustness. The solution here implemented focuses on the last 150 points per each cluster to improve the contouring in the neighborhood of the gap points.

Then, the following algorithm is applied to the obtained points from the k-means clustering algorithm. Two circles are fitted, one per each cluster. Starting from the innermost three points, a least-square circle is fitted. Then, iteratively, points are added one by one, and the fit is evaluated again. Eventually, a set of least-square fitted circles are available, and the one associated with the minimum RMSE is chosen. This condition maximizes the number of measured and clustered points within a 95% confidence level in the neighborhood of the average fit, as depicted by Figure 16.

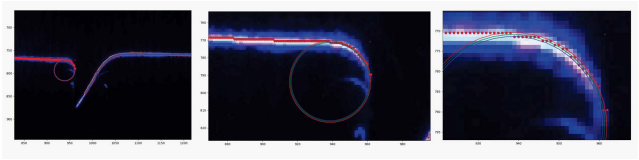

FIGURE 16. View of the circle fitting algorithm at different increasing magnification.

E. GAP AND FLUSHNESS MEASUREMENT

Gap and flushness measurement point GF, as in Figure 17, is defined relative to the radius to the center of the best-fitted circle, by summing the radius. The gap is evaluated as the difference along the x-axis between the left and right GF points. The flushness is defined as the minimum of the pair of distances computed between each GF point and the reference surface identified by the opposing metal sheet. The reference surface is evaluated by linear least-square fit of the data that are in relevant the k-means cluster, as depicted in Figure18. The reference surface is predefined factory specification that changes from measurement point to measurement point, so algorithm requires an a-priori knowledge of those reference surfaces.

IV. SYSTEM CALIBRATION

The gap and flushness evaluated according to the methodology described in Section 3.5, are still in pixel coordinates. A calibration of the non-contact machine vision system is necessary to provide a scale factor to convert pixel to metric units.

Direct calibration method is used to map the lateral and vertical variation onto the pixel coordinates [30], [31]. The laser cut of the metal sheet is designed as in Figure 19Gap and Flushness measurement point GF in order to calibrate the camera. The stripes are 4 mm thick with a variable distance between each other with minimum 0.1 mm and 10 mm, respectively.

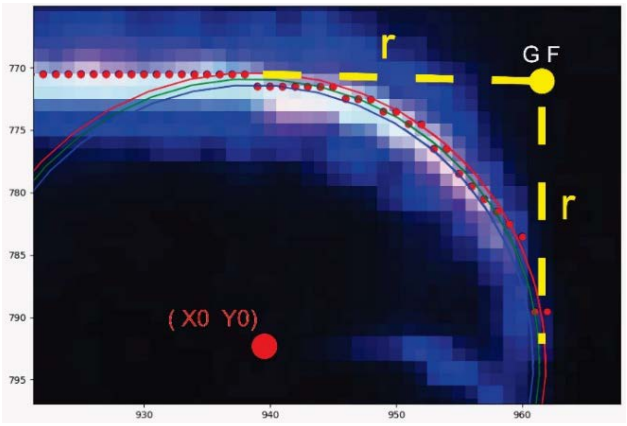

FIGURE 17. Gap and flushness measurement point GF.

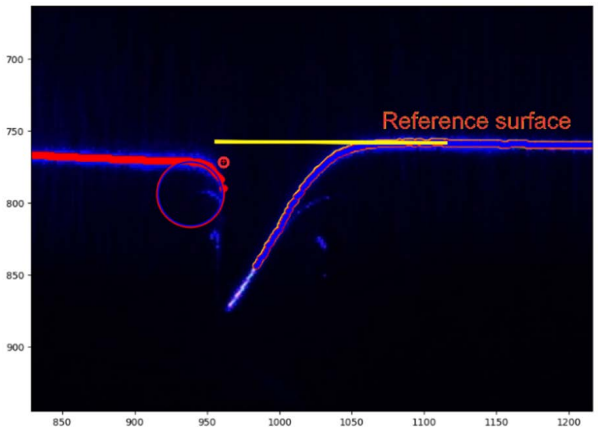

FIGURE 18. Gap and flushness measurement point GF.

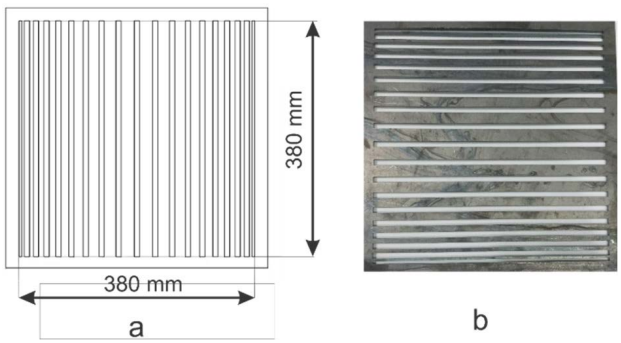

FIGURE 19. Gap and flushness measurement point GF.

The steel plate is measured with the Hexagon DEA CMM with the accuracy of 2.5 μm. The uncertainty in vertical direction is estimated by fixing on the axis a caliper with a resolution of 0.01 mm.

Gap and flushness system calibration is performed with the laser line orthogonal to the flat steel plate artefact surface and taking the pictures while increasing their distance. The calibration methodology has been described by Minetti *et al.* [21], and it is here summarized. With the considered hardware set-up, as per Section 2, increasing the

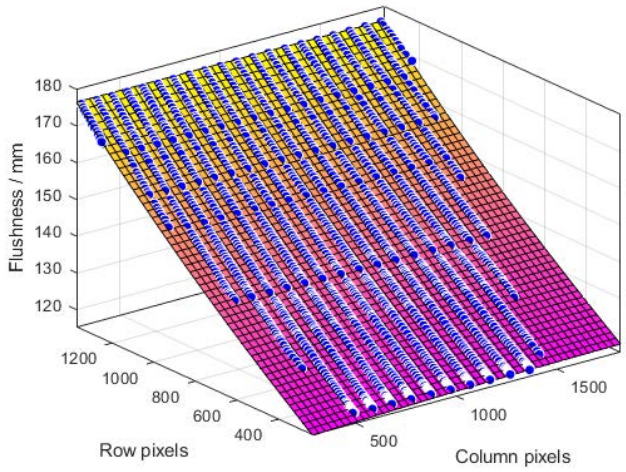

FIGURE 20. 2nd order polynomial fit derived from data on the pixels and real measurement.

distance between the camera and the surface produces a shift of the location of the laser within the field of view (FOV) of the camera. Accordingly, taking several pictures at different known distances, thanks to the calibrated scale on the vertical distance axis, allows establishing a relationship between the line laser position in the FOV, i.e. (x,y) pixels pairs, to the vertical axis position. Such relationship allows estimating distances on the vertical axis, when the images at different distances are taken, from the relative position of the line laser lines in the relevant FOVs. This enables the calibration of the scale factor on the vertical axis, that is required for the flushness measurement. In fact, as the laser line is always in the FOV of the camera and the camera is positioned always in the same orientation with respect to laser, the laser line points in the image enable the calibration of the vertical scale.

As far as the lateral dimension calibration is concerned, it is relevant remembering that the FOV has a constant dimension of (2590 × 1942) pixel, whilst the pixel dimension increases by increasing the distance between the camera and the surface. The steel plate artefact is measured by taking images at different distances between the camera and the surface. This yields images where the calibrated artefact dimensions change at different distances. Specifically, the greater the distance, the smaller the pixel dimension of the artefact features. By establishing a relationship between the calibrated feature dimension and the measured pixel dimension, the horizontal axes scale conversion factor can be calibrated. It is worth mentioning that the procedure can be carried out with a single set of measurements and that the vertical axis calibration allows inferring an intertwined relationship between the location of the laser line in the FOV, the vertical position and the lateral axes scale factor, by means of a least-square regression. Accordingly. the data are collected, and polynomial fit of 2nd order is created as in Figure 20.

The standard uncertainty of calibration is computed based on the residuals of the experimental data and polynomial fit function, which have a root mean square error of $u_{cal,G} = 0.0494$ mm and $u_{cal,F} = 0.0688$ mm for gap and flushness surfaces, respectively. Ultimately, there are the standard uncertainties to be composed with the traceability contribution, according to:

$$u_{Tr} = \sqrt{u_{cal}^2 + u_{trac}^2}. \tag{8}$$

The traceability contribution for the two axes (vertical and horizontal) calibration may be well represented by the resolution contribution of caliper and the accuracy of the CMM. These are, respectively, $u_{trac,F} = 0.00289$ mm and $u_{trac,G} = 0.0025$ mm, estimated associating a uniform distribution to the resolution, according to Guide to the Expression of Uncertainty in Measurement (GUM) [32].

Therefore, the total standard uncertainty associated with calibration procedure for gap is $u_{Tr,G} = 0.0495$ mm, while the flushness accounted for $u_{Tr,F} = 0.0689$ mm. In terms of this sole scale conversion factor calibration contribution the system is apt for the measurement task at hand, for it they have a standard uncertainty smaller than the one associated to the resolution of conventionally used feeler gauges, i.e., a resolution of 0.25 mm yielding a standard uncertainty of 0.072 mm.

V. SYSTEM METROLOGICAL CHARACTERIZATION AND VALIDATION

A. EVALUATION OF MEASUREMENT UNCERTAINTY

The expanded measurement uncertainty has to be evaluated to metrologically characterize the system and to enable the comparison with the conventional measurement methods currently adopted in production and to verify adequacy of the proposed method to measure within specification tolerances. The method used is the practical tool of Measurement Systems Analysis (MSA) to obtain the measuring process uncertainty according to the Guide to the Expression of Uncertainty in Measurement (GUM) [32]. The combined uncertainty is calculated based on calibration uncertainty, repeatability and reproducibility. The total calibration uncertainty is evaluated in Section IV. Repeatability and reproducibility are evaluated by means of one set of test via the Gauge Repeatability and Reproducibility (Gauge R&R) study [33], which exploits Analysis of Variance (ANOVA) [30].

The factors considered in the performed gauge R&R experiments [30], are the robot path in measuring the sequence of the considered measurement points and the measurement points. Respectively, 3 different paths were considered and programmed for the robotic arm, and 15 measurement points were considered, shown in Figure 21. Per each measured point, 3 replicated measurements per each path were performed. Accordingly, in total, 9 measurements per each of the 15 measurement points were performed, yielding an overall dataset size of 135 measurements.

The following influence factors should be considered:

- The total traceability contribution, from calibration $\sigma_{Tr}^2 = u_{Tr}^2$;

- Measurement system variability $\sigma^2_{measurementerror}$.

These are combined as:

$$\sigma^2_{Tot} = \sigma^2_{Tr} + \sigma^2_{measurementerror}, \tag{9}$$

having σ^2_{Tot} is the total variance of the system, while the gauge R&R focuses on $\sigma^2_{measurement\ error}$ that is equal to the sum of reproducibility and repeatability components:

$$\begin{aligned}\sigma^2_{Measurement\ Error} &= \sigma^2_{Gauge} \\ &= \sigma^2_{Repeatability} + \sigma^2_{Reproducibility}\end{aligned} \tag{10}$$

The gauge R&R analysis is performed on the commercial software MINITAB 17. The expanded measurement uncertainty of the system is evaluated considering the coverage factor k, according to GUM, assuming that the squared root of the total variance estimates the combined standard uncertainty:

$$U = k \cdot u_{Tot} = k \cdot \sigma_{Tot}. \tag{11}$$

As far as the gap measurement is concerned, the uncertainty contributions are the gauge R&R, $\sigma_{Gauge,G} = 0.0990$ mm and the calibration standard uncertainty $\sigma_{Tr,G} = 0.04946$ mm. These yield a combined standard uncertainty of $u_{Tot,G,N-C} = 0.1107$ mm. With a coverage factor $k = 2$, i.e., 95% confidence level, it results $U_{N-C,G} = 0.2214$ mm expanded uncertainty for the proposed non-contact system.

As far as the measurement uncertainty of flushness measurement is concerned, the total gauge R&R contribution is $\sigma_{Gauge,F} = 0.0056$ mm, with a calibration contribution $\sigma_{Tr,F} = 0.069$ mm. Thus, the combined standard uncertainty results of $u_{Tot,F,N-C} = 0.0887$ mm. Provided a conventional confidence level of 95%, the flushness expanded uncertainty is $U_{N-C,F} = 0.177$ mm.

The gauge R&R analysis ANOVA identifies, as expected, as the only significant factor introducing differences on the measurement averages the points, whilst the tool path and their interaction are not significant with a risk of error of 5%. Figure 22 and Figure 23 show details of the gauge R&R analysis for the gap and the flushness, respectively. According to the previous discussion, the greater contribution to overall variability is ascribed to the measured points. Control charts the average value ($\bar{x}$) and the range (R) provide insights on the metrological properties of the system. The $\bar{x}$ chart shows that for both the gap and the flushness all the points are outside the specification limits of the chart, computed according to the repeatability and reproducibility of the system [33]. Thus, the system is capable of identifying different measured points as diverse entities, as expected. The R-chart shows that all points, but for few exceptions fall inside the specification limits, i.e., it is in control. Therefore, the system is capable of managing the random variability of the measurand [33].

The evaluated expanded measurement uncertainty allows the verification of the proposed non-contact measurement system with respect the required factory specification limits. Table 1 reports the specification limits of the surface

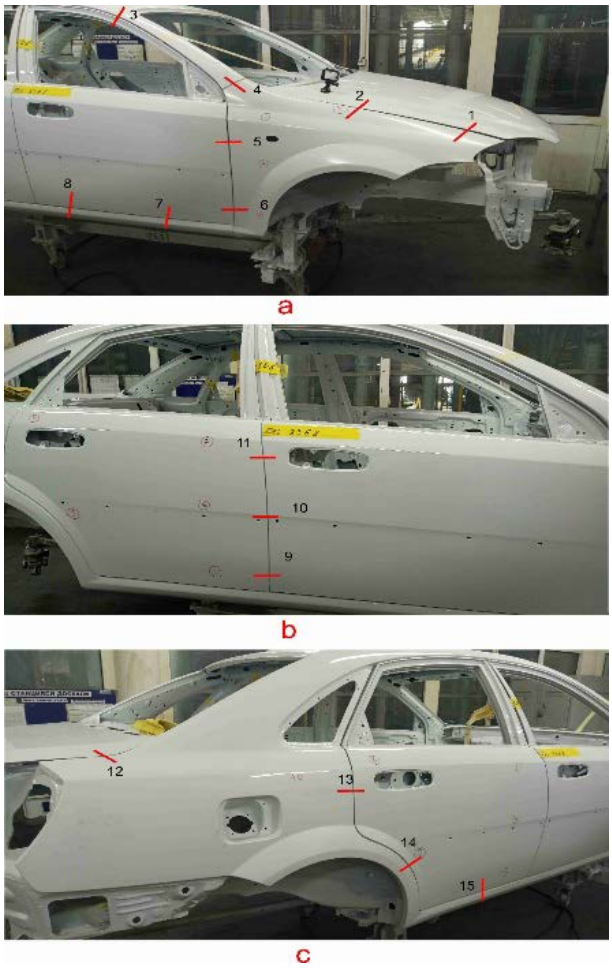

FIGURE 21. Measured car body: a) Front part with measurement points from 1 to 8 b), middle points from 9 to 11, c) back of the body with points from 12 to 15.

characteristics to be measured based on the factory standard tolerance specifications. As it can be noticed, tolerances are in the most stringent case of ±0.25 mm for both the gap and the flushness. Uncertainty and tolerance specification limits are compared according to ISO 14253-1:2017 [34], and metrological performances of the designed system compliance with tolerance specification limit to enable adequate conformity verification is satisfied for all the points. In particular, the specification zone width, T, when deduced of a bilateral guard band, GB, proportional to the standard combined uncertainty, u_{Tot}, by a guard band factor, g, must still be positive to allow a non-null acceptance zone width, A, i.e.:

$$A = T - G_B = (USL - LSL) - 2g \cdot u_{Tot} > 0 \tag{12}$$

where USL and LSL are the upper and lower specification limit, respectively.

The guard band factor is inversely dependent on the T/u_{Tot} ratio, so that for the $T/u_{Tot} < 4$, g ~ 2 and for $T/u_{Tot} > 5$, g ~ 1.65 [34]. Since u_{Tot} is fixed for gap and flushness, it is sufficient to verify condition of (12) only for the narrowest specification zone, i.e., for the smallest T.

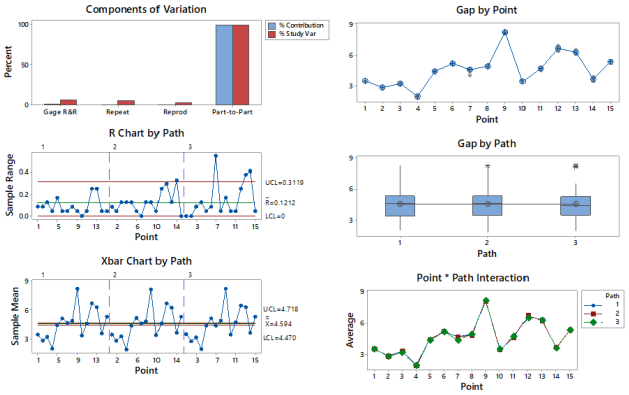

FIGURE 22. Details of gauge R&R analysis for gap measurement.

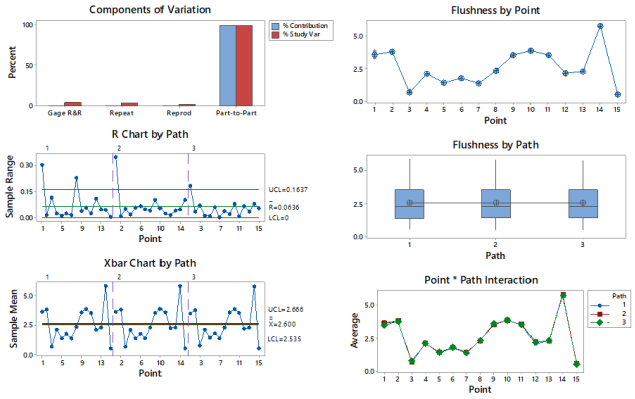

FIGURE 23. Details of gauge R&R analysis for flushness measurement.

Table 2 reports the results of such verification, which, as it can be seen, is satisfied, thus demonstrating the suitability for the considered measurement task of the proposed non-contact measurement system.

B. SYSTEM VALIDATION

In order to validate the measurement system, a comparison of obtained results by the designed non-contact inspection system with reference values is addressed.

The same aforementioned 15 measurement points were measured, again, by the non-contact system considering only 1 robot path and 10 replications. The reference measurement is provided by 10 replicated measurements of each performed by a highly experienced operator by the use of a caliper with 0.01 mm resolution. It is relevant to stress that the measurement procedure to gather the reference values is highly impractical, although highly precise, and therefore it is not used in production. Other alternative measurement methods, actually used, e.g. feeler gauges, would result, on the other hand, too uncertain.

The comparison is performed by means of a hypothesis test on the difference of the samples set averages [30], [35]. Let, $p \in \{1, \ldots, 15\} \subseteq \mathbb{N}$ the subscript indicating the p-th measurement point. According to the experimental procedure described above, per each measurement point's gap and

TABLE 1. Factory standard tolerance specification limits for gap and flushness of the 15 measured points.

Point	GAP [LSL; USL] / mm	FLUSHNESS [LSL; USL] / mm
1	[2.5;4.0]	[-0.3;0.7]
2	[2.5;4.0]	[-0.3;0.7]
3	[4.0;6.0]	[-0.3;0.8]
4	[2.0;3.5]	[-0.5;0.5]
5	[3.5;4.0]	[-1.0;0.0]
6	[3.5;4.0]	[-1.0;0.0]
7	[1.5;2.5]	[0.0;0.5]
8	[1.5;2.5]	[0.0;0.5]
9	[3.0;5.0]	[0.0;1.0]
10	[3.0;5.0]	[0.0;1.0]
11	[3.0;5.0]	[0.0;1.0]
12	[2.5;4.0]	[-0.3;0.7]
13	[4.0;6.0]	[0.0;1.0]
14	[4.0;6.0]	[0.0;1.0]
15	[4.0;6.0]	[0.0;1.0]

TABLE 2. Verification of measurement system conformity with tolerance specification.

	T / mm	g / -	A / mm
Gap	0.5	1.68	0.128
Flushness		1.65	0.207

flushness, two sets of 10 data are collected, $d_{N-C,p}$ and $d_{C,p}$, respectively with the non-contact measurement system and the caliper. Empirical means of the two data sets, $\overline{d_{N-C,p}}$ and $\overline{d_{C,p}}$ can be computed and the average difference results:

$$\overline{\delta_p} = \overline{d_{N-C,p}} - \overline{d_{C,p}}. \tag{13}$$

The hypothesis test is based on the t-Student distribution with null (H_0) and alternative (H_1) hypotheses:

$$H_0 : \overline{d_{N-C,p}} = \overline{d_{C,p}} \Leftrightarrow \overline{\delta_p} = 0 \tag{14.1}$$
$$H_1 : \overline{d_{N-C,p}} \neq \overline{d_{C,p}} \Leftrightarrow \overline{\delta_p} \neq 0 \tag{14.2}$$

The hypothesis test is performed at a confidence level of 95%, accordingly, the hull hypothesis is rejected if the test statistic $\overline{\delta_p}$ does not belong to the confidence interval, i.e.

$$if\, \overline{\delta_p} \notin C.I. = \left\{ t_{18,0.025} s_{\overline{\Delta_p}}, t_{18,0.975} s_{\overline{\Delta_p}} \right\} \Rightarrow reject\ H_0 \tag{15.1}$$

$$s_{\overline{\Delta_p}} = \frac{\sqrt{u^2_{Tot,N-C} + u^2_{Tot,C}}}{\sqrt{10}} \tag{15.2}$$

with $s_{\overline{\Delta_p}}$ the pooled standard deviation of the average difference.

Applying the gauge R&R methodology for caliper measurements, considering 3 operators and 3 replications per

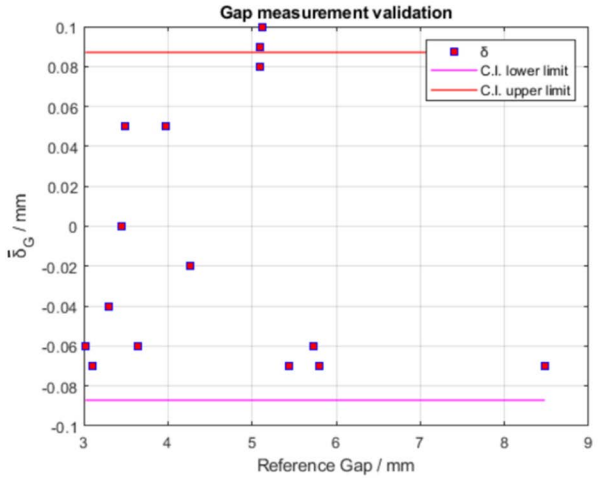

FIGURE 24. Validation of gap measurement: t-test graphical representation at 95% confidence level.

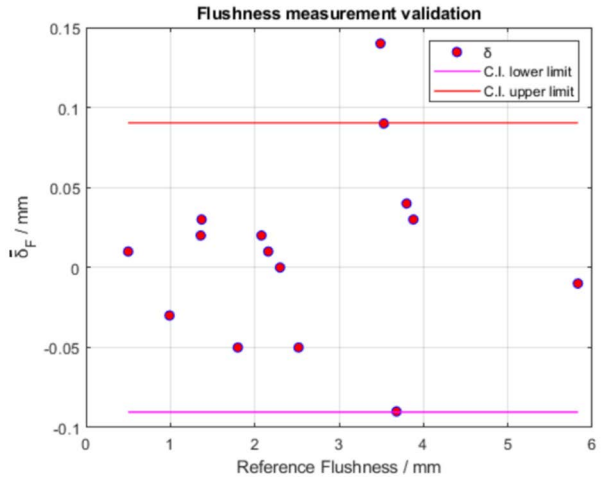

FIGURE 25. Validation of flushness measurement: t-test graphical representation at 95% confidence.

measured point, it was obtained the standard combined uncertainty of $u_{Tot,G,C} = 0.0704$ mm and $u_{Tot,F,C} = 0.1033$ mm for gap and flushness, respectively.

The qualitative test results are shown in Figure 24 and Figure 25 for gap and flushness, respectively.

One can see from Figure 24 and Figure 25 that in real production environment some of the values are outside the confidence interval, meaning that in few cases a systematic error can be appreciated between the proposed measurement system and the reference measurement based on caliper. However, this is marginal, as it happens in 2 points out of 15 and 1 out of 15 for gap and flushness, respectively, and it could be a result of operator's error, electromagnetic noises and others.

The system accuracy is evaluated averaging the 15 measured differences. It results in $Acc_G = -0.0100$ mm and $Acc_F = 0.0107$ mm, for gap and flushness, respectively.

VI. CONCLUSION

This paper presents an innovative non-contact measurement system complemented by an improved machine-vision inspection approach that can be integrated on robotic arm for the measurement of gap and flushness in automobile assembly process. The system uses sensitive camera and 405 nm line laser projected onto the body of the vehicle. The system is aimed to eliminate the human interaction into the quality control system of the production process, while providing a robust, accurate and precise measurement system that can be available at higher competitiveness with respect to other non-contact available solutions. The methodology is based on an image processing algorithm that firstly captures the images, finds the center of the laser line and afterwards defines the extremities for gap and flushness measurement points. Then, calibration techniques enable to convert the pixel data into the real dimensions.

The proposed methodology is demonstrated to measure the car body, after the painting, inside a black room with elimination of the light source inside. In this way, we can decrease the influence of the vehicle color on the image, still preserving the amount of reflection needed for capturing the image.

The system design allows flexible deployment for different production lines, for just devoted robot programming might be required to match different size, location and paths of the points to be measured on a different vehicle model.

The system was metrologically characterized resulting in expanded uncertainty of 0.221 mm and 0.177 mm and accuracy of 0.01 mm and 0.011 mm, for gap and flushness respectively. The system measurement capability to satisfy common standard tolerance specification was tested and it was validated in real production environment, demonstrating in both cases adequate performances. An important aspect of the laser system integration into the robotic arm is the capability to cope with the stringent time scheduling requirement in the production process, while enabling full automation of the inspection process with high metrological performances. The system, despite the different light response behavior of different measured points on the car body, proved to be robust and capable of performing the measurements with satisfactory metrological and quality performances. However, the system requires an a-priori knowledge of the physical appearance of the matching sheet metal to define reference surfaces. The system will allow to product and quality engineers to collect quantitative information about the gap and flushness to help improve specification and production quality. Additionally, the gathered quantitative information might be beneficial in the case an out-of-specification point is detected. In fact, this critical condition requires strategic decision to be deployed. Typically, re-working and adjustment of the assembly are performed, where possible, e.g., adjusting the doors mounting on the BIW. In such a scenario, the availability of quantitative information might speed up the process.

Future works will achieve full automation and training of the inspection system by investigating artificial intelligence approaches to automatically detect the position on the car body portion of the measurand point and infer the type of matching elements to determine the reference surfaces.

Furthermore, the economic aspects of application of the proposed plug-and-play camera system could be significantly more attractive than other commercially available tools with an order of magnitude savings, at least. Indeed, the price difference comes along with a relevant better precision of commercially available systems. However, the metrological characterization and validation of the proposed measurement system showed adequacy in common industrial relevant environment. Moreover, it would represent a significative metrological improvement at a reasonable cost for the systems that are now used in the production, i.e., manual measurements with feeler gauges, which do not allow neither precise measurement nor to perform robust statistical analysis of the operator's measurements.

REFERENCES

[1] I. Kambarov, G. D'antonio, K. Aliev, P. Chiabert, and J. Inoyatkhodjaev, "Uzbekistan towards Industry 4.0. Defining the gaps between current manufacturing systems and Industry 4.0," in *Proc. Conf. 15th IFIP Int. Conf. Prod. Lifecycle. Manag.*, Turin, Italy, Jul. 2018, pp. 250–260.

[2] C.-H. Jun, S.-H. Lee, J. Jung, T.-S. Kim, and J.-H. Lee, "Identifying sources of dimensional variation affecting assembly quality of automobiles," in *Proc. APIEMS Conf.*, Nusa Dua, Bali, Dec. 2008, pp. 1–7.

[3] G. D'Emilia, A. Gaspari, C. Iavicoli, and E. Natale, "Measurement uncertainty estimation of gap and profile in the automotive sector," in *Proc. Conf. Journ. Phys., Conf.*, Naples, Italy, vol. 1589, Oct. 2019, Art. no. 012017.

[4] T. Pribanić, T. Petković, M. Đonlić, V. Angladon, and S. Gasparini, "3D structured light scanner on the smartphone," in *Proc. Int. Conf. Image Anal. Recognit.*, in Lecture Notes in Computer Science, vol. 9730, 2016, pp. 443–450.

[5] V. D. Hoang and K. H. Jo, "Automatic calibration of camera and LRF based on morphological pattern and optimal angular back-projection error," in *Proc. Int. J. Cont., Autom. Syst.*, Sep. 2015, pp. 1436–1445.

[6] T. T. Tran and C. Ha, "Slippage estimation using sensor fusion," in *Pro. Int. Comp. Theor. Appl.* (Lecture Notes in Computer Science), vol. 9772. Cham, Switzerland: Springer, 2016.

[7] J. Kholkhujaev, N. Abdurakhmonov, S. Ruzimov, N. Abdukarimov, J. Inoyatkhodjaev, and A. Saidov, "Ray tracing simulation of wing mirrors for ultrasonic sensor based blind spot monitoring system," in *Proc. IEEE 14th Int. Conf. Appl. Inf. Commun. Technol. (AICT)*, Oct. 2020, pp. 1–6.

[8] T. T. Trang and C. Ha, "Irregular moving object detecting and tracking based on color and shape in real-time system," in *Proc. Int. Conf. Comput., Manage. Telecommun. (ComManTel)*, Jan. 2013, pp. 415–419.

[9] R. Hartley and A. Zisserman, *Multiple View Geometry in Computer Vision*. Cambridge, U.K.: Cambridge Univ. Press, 2004.

[10] M.-H. Le, H.-H. Trinh, V.-D. Hoang, and K.-H. Jo, "Automated architectural reconstruction using reference planes under convex optimization," *Int. J. Control, Autom. Syst.*, vol. 14, no. 3, pp. 814–826, Jun. 2016.

[11] Y. S. Suh, N. H. Q. Phuong, and H. J. Kang, "Distance estimation using inertial sensor and vision," *Int. J. Control, Autom. Syst.*, vol. 11, no. 1, pp. 211–215, Feb. 2013.

[12] D. Kosmopoulos and T. Varvarigou, "Automated inspection of gaps on the automobile production line through stereo vision and specular reflection," *Comput. Ind.*, vol. 46, no. 1, pp. 49–63, Aug. 2001.

[13] J.-K. Oh, S. Lee, and C.-H. Lee, "Stereo vision based automation for a bin-picking solution," *Int. J. Control, Autom. Syst.*, vol. 10, no. 2, pp. 362–373, Apr. 2012.

[14] *8 SIT: Portable Inspection Tool for Assessing Gap & Flush on the Car Body—GO0D MAN Innovation Shop*. Accessed: Mar. 18, 2022. [Online]. Available: https://go0dman.boc-group.eu/innovationshop/projects/08_SIT_Gap_Flush/

[15] *Measure Gap and Flush With Leading Laser Measurement Tool, Gap-Gun*. Accessed: Mar. 18, 2022. [Online]. Available: https://www.third.com/products/hardware/gapgun/

[16] *Automation Syst.—LaserGauge? | LMI Corporation*. Accessed: Mar. 18, 2022. [Online]. Available:. https://origintech.com/products/automation-system

[17] *Measuring Equipment & Inspection Systems| Home—NEXTSENSE*. Accessed: Mar. 18, 2022. [Online]. Available: https://www.nextsense-worldwide.com/en/home.html

[18] T.-T. Tran and C. Ha, "Non-contact gap and flush measurement using monocular structured multi-line light vision for vehicle assembly," *Int. J. Control, Autom. Syst.*, vol. 16, no. 5, pp. 2432–2445, Oct. 2018.

[19] L. H. Pham, D. N.-N. Tran, J. Y. Byun, C. H. Rhie, and J. W. Jeon, "A smartphone-based laser measuring system for gap and flush assessment in car body," in *Proc. Conf. IEEE Trans. Ind. Electron.*, Jul. 2021, vol. 68, no. 7, pp. 6297–6307.

[20] E. Minnetti, P. Chiariotti, N. Paone, G. Garcia, H. L. V. Violini, and P. Castellini, "A smartphone integrated hand-held gap and flush measurement system for in line quality control of car body assembly," *Sensors*, vol. 20, no. 11, pp. 1–17, Jun. 2020.

[21] I. Zeger, S. Grgic, J. Vukovic, and G. Sisul, "Grayscale image colorization methods: Overview and evaluation," *IEEE Access*, vol. 9, pp. 113326–113346, 2021.

[22] A. K. Jain and R. C. Dubes, *Algorithms for Clustering Data*. Englewood Cliffs, NJ, USA: Prentice-Hall, 1988.

[23] G. Barbato, E. M. Barini, G. Genta, and R. Levi, "Features and performance of some outlier detection methods," *J. Appl. Statist.*, vol. 38, no. 10, pp. 2133–2149, Oct. 2011.

[24] G. Maculotti, G. Genta, D. Quagliotti, M. Galetto, and H. N. Hansen, "Gaussian process regression-based detection and correction of disturbances in surface topography measurements," *Qual. Rel. Eng. Int.*, vol. 38, no. 3, pp. 1501–1518, Apr. 2022.

[25] D. S. Lavrinov and A. I. Khorkin, "Problems of internal calibration of precision laser triangulation 2D scanners," in *Proc. 2nd Int. Conf. Ind. Eng., Appl. Manuf. (ICIEAM)*, 2016, pp. 1–4, doi: 10.1109/ICIEAM.2016.7910962.

[26] W. Burger and M. J. Burge, *Undergraduate Topics in Computer Science*. London, U.K.: Springer-Verlag, 2009.

[27] G. Maculotti, N. Senin, O. Oyelola, M. Galetto, A. Clare, and R. Leach, "Multi-sensor data fusion for the characterisation of laser cladded cermet coatings," in *Proc. 19th Int. Conf. Exhib. Eur. Soc. Precis. Eng. Nanotechnol., Conf.*, Jun. 2019, pp. 260–263.

[28] H. Abdul-Rahman and N. Chernov, "Fast and numerically stable circle fit," *J. Math. Imag. Vis.*, vol. 49, no. 2, pp. 289–295, Jun. 2014.

[29] D. C. Montgomery, *Introduction to Statistical Quality Control*, 7th ed. New York, NY, USA: Wiley, 2009.

[30] E. Trucco, R. B. Fisher, and A. W. Fitzgibbon, "Direct calibraction and data consistency in 3-D laser scanning," in *Proc. Brit. Mach. Vis. Conf.*, vol. 2, 1994, pp. 489–498.

[31] *Evaluation of Measurement Data—Guide to the Expression of Uncertainty in Measurement (GUM)*, document JCGM 100:2008, Sep. 2008.

[32] D. C. Montgomery, *Design and Analysis of Experiments*. New York, NY, USA: Wiley, 2009.

[33] *Geometrical Product Specifications (GPS)—Inspection by Measurement of Workpieces and Measuring Equipment—Part 1: Decision Rules for Verifying Conformity or Nonconformity With Specifications*, Standard ISO 14253-1:2017, 2017.

[34] G. Maculotti, E. Goti, G. Genta, L. Mazza, and M. Galetto, "Uncertainty-based comparison of conventional and surface topography-based methods for wear volume evaluation in pin-on-disc tribological test," *Tribol. Int.*, vol. 165, Jan. 2022, Art. no. 107260.

JASURKHUJA KHOLKHUJAEV received the M.Sc. degree in mechatronics engineering from Turin Polytechnic University in Tashkent, Uzbekistan, in 2017. He is currently pursuing the Ph.D. degree in management, production and design. He is currently an Exchange Ph.D. Student at the Department of Management and Production Engineering (DIGEP), Politecnico di Torino. His current research interests include visual inspection, industrial metrology, machine vision, and quality engineering.

GIACOMO MACULOTTI received the M.Sc. degree in automotive engineering and the Ph.D. degree in management, production and design from the Politecnico di Torino, Italy, in 2017 and 2020, respectively. He is currently a Research Fellow at the Department of Management and Production Engineering (DIGEP), Politecnico di Torino. His current research interests include industrial metrology, technological surfaces characterization, and quality engineering.

GIANFRANCO GENTA received the M.Sc. degree in mathematical engineering and the Ph.D. degree in metrology: measuring science and technique from the Politecnico di Torino, Italy, in 2005 and 2010, respectively. He is currently an Associate Professor at the Department of Management and Production Engineering (DIGEP), Politecnico di Torino, where he teaches "Design of Industrial Experiments," "Experimental Statistics and Mechanical Measurement," and "Quality and Measurements Management Laboratory." He is a Research Affiliate of The International Academy for Production Engineering (CIRP) and a fellow of the Associazione Italiana di Tecnologia Meccanica (A.I.Te.M.). He has authored and coauthored three books and more than 70 publications on international journals and conference proceedings. His current research interests include industrial metrology, quality engineering, and experimental data analysis.

MAURIZIO GALETTO received the M.Sc. degree in physics from the University of Turin, Italy, in 1995, and the Ph.D. degree in metrology: measuring science and technique from the Politecnico di Torino, Italy, in 2000. He is currently a Full Professor and the Head of the Department of Management and Production Engineering (DIGEP), Politecnico di Torino, where he teaches "Quality Engineering" and "Experimental Statistics and Mechanical Measurement." He is also an Associate Member of The International Academy for Production Engineering (CIRP) and a fellow of the Associazione Italiana di Tecnologia Meccanica (A.I.Te.M.) and the European Network for Business and Industrial Statistics (ENBIS). He has authored and coauthored four books and more than 100 published papers in scientific journals, and international conference proceedings. At present, he collaborates in some important research projects for public and private organizations. His current research interests include quality engineering, statistical process control, industrial metrology, and production systems. He is a Member of the Editorial Board of the scientific international journal *Nanomanufacturing and Metrology* and collaborates as a referee for many international journals in the field of industrial engineering

JAMSHID INOYATKHODJAEV received the M.Sc. degree in internal combustion engines from the Tashkent Automobile and Road construction Institute, in 2005, the Ph.D. degree in 2009, and the D.Sc. degree in automotive engineering, in 2017. He is currently a Rector of Turin Polytechnic University in Tashkent and the Head of the Scientific Council of University. At present, he collaborates in some important research projects for public and private organizations. His current research interests include quality engineering, automobile engineering, internal combustion engine engineering, manufacturing process, and production systems.